Cryogenically formed discharge waveguide

K. K. Swanson,[1,2] A. J. Gonsalves[1,*] H.-S. Mao,[3] T. Sipla,[1] S. S. Bulanov,[1] N. A. Bobrova,[3]
P. V. Sasorov,[3,4] G. Korn,[4] C. Benedetti,[1] C. V. Pieronek,[1,2] C. B. Schroeder,[1,2]
C. G. R. Geddes,[1] E. Esarey,[1] and W. P. Leemans[1,2,5]

[1]*Lawrence Berkeley National Laboratory, 1 Cyclotron Rd, Berkeley, California 94720, USA*
[2]*University of California–Berkeley, Berkeley, California 94720, USA*
[3]*Keldysh Institute of Applied Mathematics, Moscow 125047, Russia*
[4]*Institute of Physics ASCR, v.v.i. (FZU), ELI-Beamlines, 182 21 Prague, Czech Republic*
[5]*Deutsches Elektronen Synchrotron, Notkestraße 85 22607 Hamburg, Germany*

We describe the development and operation of a regenerative, cryogenically-formed discharge waveguide formed by freezing nitrous oxide gas onto the inner wall of a sapphire capillary. We demonstrate a technique for varying the channel diameter *in situ* and present guiding of low-power laser pulses through 6-cm long waveguides with channel diameters of 0.7, 0.8, and 1 mm. Measurements and simulations of the output laser fluence showed that the matched spot size could be adjusted with the thickness of the solid nitrous oxide layer.

With the expanding number of petawatt-class laser systems [1–3] and recent advances in laser plasma accelerators (LPAs) [4–6], there is an increased interest in using novel accelerating structures as a source of energetic particles for applications including high-energy physics, free-electron lasers, and sources of THz and x-ray radiation [7–14]. For many of these applications, optical guiding is required to keep the laser intense over extended distances. Without any form of guiding, the interaction length is typically limited by diffraction to the Rayleigh length $Z_R = \pi w_0^2 / \lambda$, where w_0 is the laser spot size and λ is the laser wavelength.

To counteract laser diffraction and propagate a pulse over many Rayleigh lengths, thus increasing the final particle beam energy, various waveguides have been developed [15–21]. In a gas-filled capillary discharge waveguide, a discharge pulse heats and ionizes gas inside the channel to form a plasma which develops a radial temperature gradient as heat flows from the hot plasma center to the cold capillary wall [22–30]. This temperature gradient produces a density distribution with an approximately parabolic radial profile of the form $n_e(r) = n_e(0) + n_e''(0)r^2/2$. A low-power transversely Gaussian laser pulse can propagate

with constant spot size and intensity if the input laser spot size equals the matched spot size

$$w_m = \left(\frac{2}{\pi r_e n_e''(0)} \right)^{1/4}, \qquad (1)$$

where r_e is the classical electron radius. If the input spot size is not matched to the channel, the spot size will oscillate as the laser propagates. In a capillary discharge waveguide, once the plasma reaches equilibrium, the matched spot size scales with the average density n_e and capillary radius r_{cap} as $w_m \propto n_e^{-1/4} r_{cap}^{1/2}$ [28].

The maximum particle energy gain achievable in a single laser plasma accelerator stage scales with the plasma density as n_e^{-1}. Guiding of pulses with peak intensity of 5×10^{18} W/cm^2 has been demonstrated in a 9-cm long capillary discharge waveguide with a plasma density of approximately 7×10^{17} cm^{-3}, accelerating electron beams up to 4.2 GeV [31]. Further increases in beam energy can be achieved by decreasing the plasma density. However, a smaller capillary radius is required to maintain matched guiding at a lower density, leading to damage as the wings of the laser pulse interact with the channel entrance and walls. Instead, a channel with a larger radius can guide a laser pulse if the depth of the density profile $n_e''(0)$ is increased. By coupling a nanosecond-scale laser pulse into a capillary discharge waveguide, the plasma can be additionally heated through inverse-bremsstrahlung absorption [32]. This heating reduces the density on axis and creates a stronger channel capable of guiding pulses with a smaller matched spot size. Guiding of pulses with intensities

*ajgonsalves@lbl.gov

up to 10^{19} W/cm^2 has been demonstrated in a 20-cm long capillary discharge waveguide, accelerating electron beams up to 7.8 GeV with a plasma density of 3×10^{17} cm^{-3} [6,33,34]. However, to further increase the beam energy, a reduction in the plasma density is again required, leaving the capillary susceptible to damage.

In this paper, we report the development and operation of a regenerative, variable-radius, cryogenically-formed waveguide. The design of the waveguide enables *in situ* adjustment of the channel radius, allowing for improved laser guiding. The ability to regenerate the waveguide allows for a wide range of channel diameters to be explored while alleviating the problem of laser damage, increasing the waveguide lifetime.

The waveguide was a modified 6-cm long and helium-filled capillary discharge waveguide with a 1-mm diameter channel laser machined into sapphire plates. Two slots 1 mm in diameter were machined 6 mm from the ends of the sapphire plates and introduced gas into the central channel. Using liquid nitrogen, the sapphire plates were cooled at a rate of 1.5 K/s. The temperature was measured by a thermocouple attached to an outside wall of the sapphire. Once the temperature reached 155 K, nitrous oxide (N$_2$O) gas controlled by a pulsed valve was flowed through the gas slots into the central channel for up to 2.2 s with a backing pressure of 10 psi. At this wall temperature, the gas deposited onto the inside wall of the channel, forming a stable shell of solid N$_2$O.

The thickness and uniformity of the solid N$_2$O shell along the length of the center of the channel, between the gas slots, was measured by a Thorlabs spectral-domain optical coherence tomography system with a 5 μm axial resolution. The capillary was imaged using two $f = 200$ mm, 2 in. diameter achromatic lenses. A schematic of the setup is shown in Fig. 1(a).

In this design, longitudinally uniform solid N$_2$O shells were achieved only at a wall temperature of 155 ± 2 K. At a higher temperature, the nitrous oxide gas would not deposit onto the channel wall. In addition, because the entire sapphire plate was cooled, deposition also occurred inside the gas slots. At a wall temperature much lower than 155 K, gas deposited inside the slots at a much faster rate than inside the central channel which resulted in longitudinally nonuniform shells and eventually blockage of the slots.

The duration of the N$_2$O gas flow through the capillary as set by the opening time of the pulsed valve determined the thickness of the solid layer: the longer the duration of the gas flow, the thicker the solid N$_2$O shells (see Supplemental Materials [35]). The inset in Fig. 1(b) shows an example longitudinal measurement of the shell thickness between the gas slots for a valve opening time of 1.5 s, resulting in a 111 ± 7.5 μm thick shell. The thickness is defined as a moving average over successive 60 μm increments to smooth out small-scale fluctuations in the
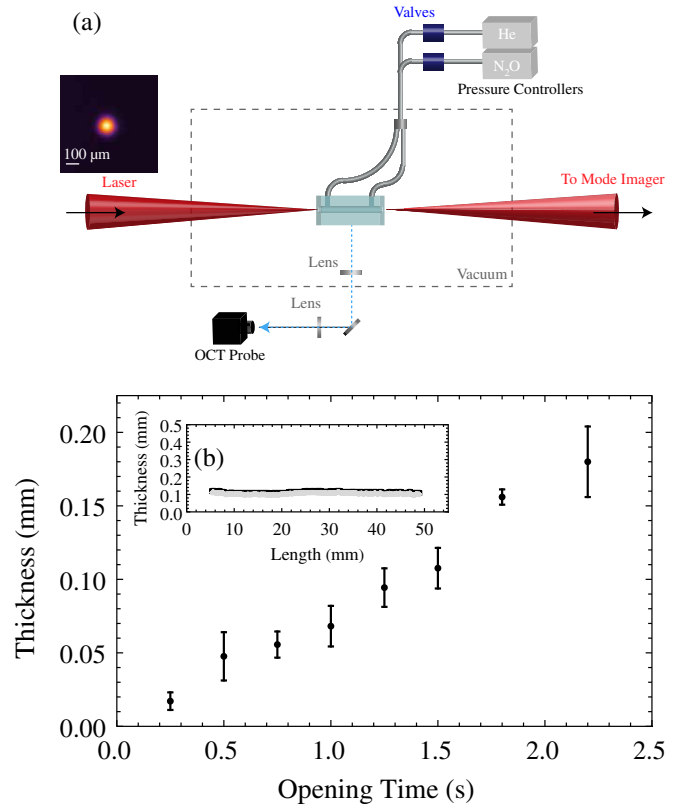

FIG. 1. (a) Schematic of the laser guiding and optical coherence tomography system setup. (b) Average thickness of the solid N$_2$O shell as a function of the pulsed valve's opening time. The error bars correspond to fluctuations in the measured thickness as a result of surface roughness. The inset shows the longitudinal thickness between the gas slots for an opening time of 1.5 s. The gray shaded region represents fluctuations in the measured thickness as a result of surface roughness.

thickness caused by surface roughness. By adjusting the opening time of the pulsed valve from 0.25 to 2.2 s, solid shells with thicknesses varying from 50 to 180 μm were reproducibly deposited [see Fig. 1(b)]. The N$_2$O shell thickness increased at a rate of 67 μm/s the pulsed valve was open. The maximum shell thickness was limited by deposition inside the gas slots which prevented gas flow into the central channel. Reduced heat transfer between the gas and the sapphire through improvements such as thermally isolating the gas slots can help mitigate this problem, allowing thicker shells and smaller channel diameters to be realized.

Once the solid N$_2$O layer formed, the capillary was filled with 20 Torr of helium gas. Two stainless steel electrodes at each end of the capillary, separated from the sapphire by approximately 0.5 mm to prevent a decrease in the electrode temperature, provided a voltage differential along the length of the capillary. A 17-kV pulser system caused the helium gas to breakdown, and a damped, approximately sinusoidal current pulse flowed through the capillary with

500 A maximum current and 320 ns quarter period. The discharge evenly ablated the solid N_2O at a rate of approximately 50 nm/shot for the thicknesses tested. Allowing more N_2O gas to flow through the channel enabled further deposition and regeneration of the solid shell.

In order to understand the behavior of the plasma density profile inside a capillary discharge waveguide with solid N_2O walls, we performed magnetohydrodynamic simulations using the 1D code NPINCH [28]. To correctly model the capillary with a solid layer of N_2O, the description of the N_2O layer as well as the phase transition from condensed to gaseous N_2O were incorporated. The phase transition onsets were set at a spinodal curve, when the matter becomes dynamically unstable, with thermodynamically unstable states included in the equation of state. Only the first stage ionization of helium was included with a maximum ionization level of seven for nitrous oxide. The description of the N_2O layer included only the inner 10 μm, assuming that deeper layers were not affected significantly during a single shot simulation. The boundary was set to have no motion with a temperature of 100 K such that the resulting N_2O vapor pressure matched the experimentally measured vapor pressure of 0.1 Torr. The region inside the internal diameter was at first occupied by helium with a density of 4.32 μg/cm^3. The discharge was defined by the boundary condition for the azimuth component of the magnetic field, which required the total electric current through the capillary to be of the form $I(t) = I_0 \sin(\pi t/t_0)$, where $I_0 = 500$ A and $t_0 = 650$ ns.

From Fig. 2, we can see the evolution of the plasma density during the discharge for a 100 μm shell thickness. In a manner similar to the case with no solid N_2O present, a parabolic density profile forms as the helium is heated and ionized by the electrical current [28,36]. However, at approximately 100 ns before the peak of the current the ablation of the N_2O layer starts. A fraction of the ablated material forms a cold, dense, and almost neutral gas layer of about 22 μm thick on top of the shell. This layer has $T_e \gg T_i$ and is slightly ionized (the degree of ionization varies from 10^{-4} to 0.1). The ablated N_2O plasma then propagates inward, pushing helium toward the capillary axis and increasing in the plasma density. However, the helium plasma maintains an approximately parabolic shape near the axis. By the end of the current pulse, approximately 130 nm of the solid N_2O layer is ablated, approaching the experimentally measured ablation rate considering a fraction of the nitrous oxide will redeposit. The N_2O plasma extends up to 150 μm into the channel, and at the helium-N_2O interface, the plasma temperature is approximately 3 eV with an ionization level of 1.8. Since diffusion of different ion species is not included in the model, the interface between helium and N_2O is a sharp discontinuity.

NPINCH simulations were performed for 0 (no solid N_2O), 100, and 150 μm shell thicknesses. Using the plasma
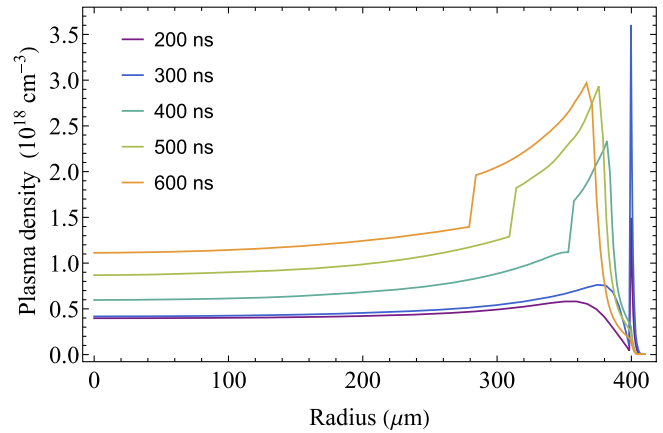

FIG. 2. Simulated radial density profiles for various times in the discharge. Discontinuities in the density are seen after 250 ns, corresponding to the contact discontinuity at the interface between the helium and N_2O plasmas.

density profile obtained in these simulations, the matched spot size was calculated for each of these channels [37]. The on axis densities and matched spot sizes are shown in Fig. 3. When no solid N_2O is present, the density is nearly uniform after the peak of current, as expected from the quasistatic equilibrium shown in previous work [28]. Correspondingly, the matched spot size is approximately constant. In contrast, in the channels with solid N_2O layers, a continuous rise in density, and thus a continuous decrease in matched spot size, is observed after the peak of the discharge current as ablated N_2O compresses the helium inside the channel. In this case, the equations for the matched spot size and density as given in Ref. [28] are not appropriate, and the scaling of the matched spot size is determined by the motion of the ablated solid N_2O-helium interface.

After 350 ns, near the peak of the discharge current, the densities in the 0 and 100 μm cases are almost identical while the matched spot sizes are 118 and 100 μm, respectively, demonstrating some tunability in the matched
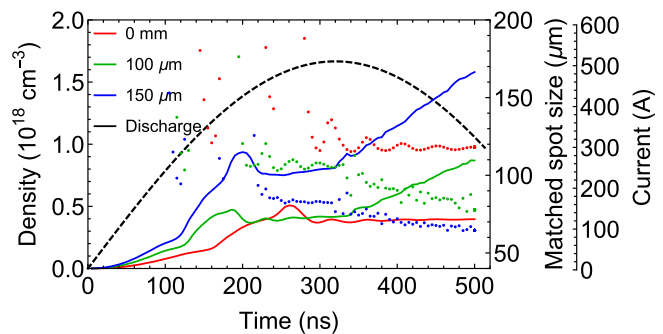

FIG. 3. Temporal evolution of the current (black, dashed line), as well as on axis density (colored lines) and matched spot size (colored points) for solid N_2O layers of thickness 0 (red), 100 (green), and 150 μm (blue).

spot size as a result of the N₂O. It should be noted that for the current used, the helium is only singly ionized, and for guiding laser pulses above the ionization threshold of the second level, it would be advantageous to either increase the current or replace the helium with hydrogen.

To study the guiding properties of the plasma channel, low-power laser pulses were propagated through the capillary. Guiding of pulses was performed using a fraction of the 1 Hz repetition rate, Ti:sapphire-based BELLA petawatt laser [38], providing pulses with 785 nm central wavelength, 1 ns full width at half maximum (FWHM) pulse duration, and 4 nJ on target. As shown in Fig. 1(a), the laser pulses were focused using an $f = 1.68$ m lens into the entrance of the capillary to an 87 μm FWHM beam waist for an intensity of 33 kW/cm². Laser transmitted through the capillary was imaged onto a charge-coupled device which could be translated along the beam axis to image either the entrance or the exit plane of the capillary.

Solid N₂O shells with 100 and 150 μm thicknesses were formed and compared to the case with no solid N₂O. N₂O was redeposited onto the walls of the channel every 200 shots, corresponding to a 10 μm change in thickness over the lifetime of the shell. The arrival time between the laser pulse and the discharge current was varied, and Fig. 4(a) shows representative images of the transmitted laser mode at the exit of the capillary. When the laser pulse was injected before and early in the discharge, the output spot size was large. For later times in the discharge, the spot size decreased as the plasma channel formed and guided the pulse.

The normalized peak fluence, defined as the ratio of the peak fluence at the exit plane of the capillary and at the focal plane, for the different solid N₂O shell thicknesses was measured near the peak of the discharge. Figure 4(b) shows the normalized peak fluences as well as the channel matched spot sizes. In the case of no solid N₂O, the matched spot size could be retrieved from measurements of laser centroid oscillations [39]. For the cases with solid N₂O, the low-capillary temperature introduced significant temporal jitter in the experiment that rendered that technique time-consuming. Therefore, the matched spot size was retrieved by modeling the beam propagation using the 2D cylindrical code INF&RNO [40,41]. The measured laser mode, retrieved from its vacuum propagation using a Gerchberg-Saxton algorithm, was propagated through parabolic plasma channels of different matched spot sizes. By matching the simulated laser fluences with the experiment, the matched spot sizes of the channels were obtained, and the results are also shown in Fig. 4(b).

In order to check the validity of this method, the matched spot size for the case of no solid N₂O was also retrieved using the laser centroid oscillation technique. The results obtained by the two techniques were equal to within the experimental error of ±3 μm. When the laser spot size approaches the matched spot size, the output fluence is very sensitive to the channel and thus the matched spot size.
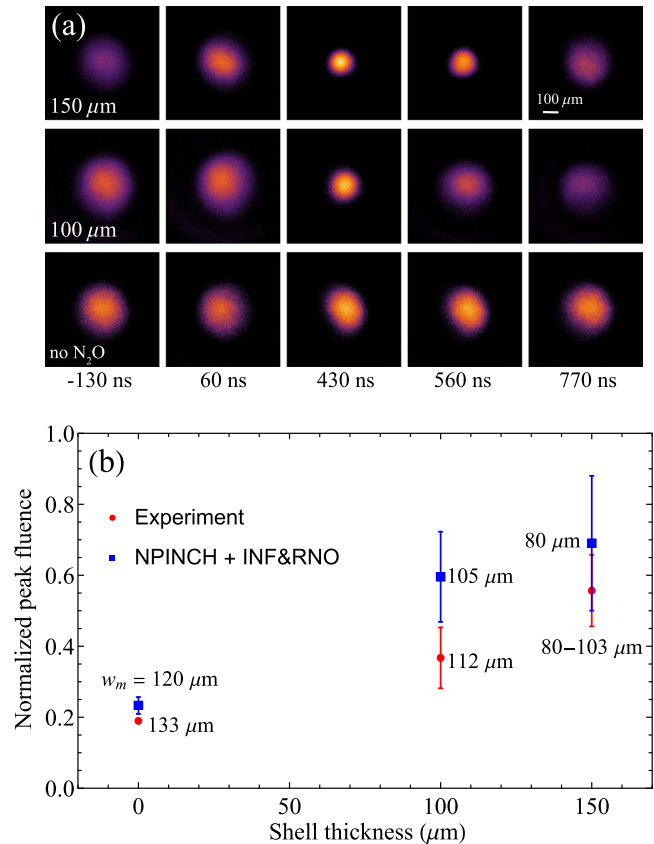

FIG. 4. (a) Representative images of the laser output mode at the exit of the capillary for 150, 100, and 0 μm shell thicknesses for discharge delays of −130, 60, 430, 560, and 770 ns. Image intensities have been normalized to the maximum intensity for that diameter. (b) Output fluence measured in the experiment (red) and simulated using the experimentally measured matched spot size (blue) as a function of shell thickness. Data were averaged for delays between 20 ns before and 60 ns after the peak of the discharge pulse. The error bars correspond to the standard deviation of the data, and the labels represent the matched spot sizes w_m. In the case of no solid N₂O, the experimental normalized peak fluence has an error of 0.006.

Therefore, there is significant ambiguity in the matched spot size in the 150-μm thick shell because of the experimental fluctuations in peak fluence. Nevertheless, it is clear that the matched spot size is reduced for increasing ice thickness as predicted in Fig. 3.

In addition, INF&RNO simulations were performed using the NPINCH density profiles and the experimentally measured laser mode. The results as shown in Fig. 4(b) demonstrate the same trend: the matched spot size decreases as the shell thickness increases. For thicker shells, simulations using the NPINCH density profiles predict higher fluences and lower matched spot sizes relative to the parabolic density profile. Further work is required to understand the differences between the two approaches which may be due to the assumptions of one-dimensional symmetry, approximations of the equations of state, or errors in

the knowledge of the initial experimental conditions. The error bars are the standard deviation of the matched spot sizes shown in Fig. 3 for times between 20 ns before and 60 ns after the peak of the discharge where there is larger variability in the matched spot size.

Here, we presented the development of a new waveguide formed by flowing N_2O gas through a capillary with walls cooled to a temperature below the freezing temperature of the gas. The nitrous oxide deposited onto the walls of the capillary, forming a stable, solid shell whose thickness was controlled by the duration of the N_2O gas flow. Channels with longitudinally uniform shell thicknesses from 50 to 180 μm were reproducibly formed. Helium flowing through the channel facilitated discharge and an approximately transverse parabolic plasma density profile developed as was corroborated by simulations and experiments. We verified *in situ* adjustment of the waveguide's matched spot size by forming solid N_2O shells with varying thicknesses and detailed a technique for regenerating ablated layers.

This waveguide has several important features for applications that require guiding of laser pulses. In a discharge capillary, the matched spot size is controlled using the channel radius and on axis density. To reach higher particle beam energies, lower plasma densities are required which, for a fixed laser spot size, necessitates a smaller channel radius. However, the capillary then becomes more susceptible to laser damage [31]. With the ability to redeposit solid N_2O onto the capillary walls, the cryogenic waveguide could operate with a longer lifetime. Additionally, the design allows for some independent control of the on axis density inside the channel using the helium gas pressure and control of the channel radius using the flow duration of the N_2O gas. Through coordination of these two parameters, better matching between the channel radius and the laser spot size could be achieved for improved guiding in a variety of different regimes. Future work will examine whether this cryogenic waveguide can be applicable as a hollow or near-hollow plasma channel.

[1]   M. Perry, D. Pennington, B. Stuart, G. Tietbohl, J. Britten, C. Brown, S. Herman, B. Golick, M. Kartz, J. Miller, H. Powell, M. Vergino, and V. Yanovsky, Opt. Lett. **24,** 160 (1999).

[2]   C. L. Haefner *et al.*, in *Society of Photo-Optical Instrumentation Engineers (SPIE) Conference Series*, Society of Photo-Optical Instrumentation Engineers (SPIE) Conference Series Vol. 10241 (International Society for Optics and Photonics, 2017), p. 1024102.

[3]   C. N. Danson, C. Haefner, J. Bromage, T. Butcher, J.-C. F. Chanteloup, E. A. Chowdhury, A. Galvanauskas, L. A. Gizzi, J. Hein, D. I. Hillier *et al.*, High Power Laser Sci. Eng. **7,** e54 (2019).

[4]   T. Tajima and J. M. Dawson, Phys. Rev. Lett. **43,** 267 (1979).

[5]   E. Esarey, C. B. Schroeder, and W. P. Leemans, Rev. Mod. Phys. **81,** 1229 (2009).

[6]   A. J. Gonsalves *et al.*, Phys. Rev. Lett. **122,** 084801 (2019).

[7]   C. B. Schroeder, E. Esarey, C. G. R. Geddes, C. Benedetti, and W. P. Leemans, Phys. Rev. ST Accel. Beams **13,** 101301 (2010).

[8]   D. Jaroszynski, R. Bingham, E. Brunetti, B. Ersfeld, J. Gallacher, B. van der Geer, R. Issac, S. Jamison, D. Jones, M. de Loos, A. Lyachev, V. Pavlov, A. Reitsma, Y. Saveliev, G. Vieux, and S. Wiggins, Philos. Trans. R. Soc., A **364,** 689 (2006).

[9]   W. P. Leemans, C. G. R. Geddes, J. Faure, C. Tóth, J. van Tilborg, C. B. Schroeder, E. Esarey, G. Fubiani, D. Auerbach, B. Marcelis, M. A. Carnahan, R. A. Kaindl, J. Byrd, and M. C. Martin, Phys. Rev. Lett. **91,** 074802 (2003).

[10] J. van Tilborg, C. B. Schroeder, C. V. Filip, C. Tóth, C. G. R. Geddes, G. Fubiani, R. Huber, R. A. Kaindl, E. Esarey, and W. P. Leemans, Phys. Rev. Lett. **96,** 014801 (2006).

[11] A. Rousse, K. T. Phuoc, R. Shah, A. Pukhov, E. Lefebvre, V. Malka, S. Kiselev, F. Burgy, J.-P. Rousseau, D. Umstadter, and D. Hulin, Phys. Rev. Lett. **93,** 135005 (2004).

[12] V. Shpakov *et al.*, Phys. Rev. Lett. **122,** 114801 (2019).

[13] J. van Tilborg, S. Steinke, C. G. R. Geddes, N. H. Matlis, B. H. Shaw, A. J. Gonsalves, J. V. Huijts, K. Nakamura, J. Daniels, C. B. Schroeder, C. Benedetti, E. Esarey, S. S. Bulanov, N. A. Bobrova, P. V. Sasorov, and W. P. Leemans, Phys. Rev. Lett. **115,** 184802 (2015).

[14] R. Pompili *et al.*, Phys. Rev. Lett. **121,** 174801 (2018).

[15] C. G. Durfee and H. M. Milchberg, Phys. Rev. Lett. **71,** 2409 (1993).

[16] S. Jackel, R. Burris, J. Grun, A. Ting, C. Manka, K. Evans, and J. Kosakowskii, Opt. Lett. **20,** 1086 (1995).

[17] M. Borghesi, A. J. Mackinnon, R. Gaillard, O. Willi, and A. A. Offenberger, Phys. Rev. E **57,** R4899 (1998).

[18] F. Dorchies, J. R. Marquès, B. Cros, G. Matthieussent, C. Courtois, T. Vélikoroussov, P. Audebert, J. P. Geindre, S. Rebibo, G. Hamoniaux, and F. Amiranoff, Phys. Rev. Lett. **82,** 4655 (1999).

[19] B. Cros, C. Courtois, G. Malka, J. R. Matthieussent, G. Marques, F. Dorchies, F. Amiranoff, S. Rebibo, G. Hamoniaux, N. Blanchot, and J. Miquel, IEEE Trans. Plasma Sci. **28,** 1071 (2000).

[20] W. P. Leemans, B. Nagler, A. J. Gonsalves, C. Tóth, K. Nakamura, C. G. R. Geddes, E. Esarey, C. B. Schroeder, and S. M. Hooker, Nat. Phys. **2,** 696 (2006).

[21] C. Mcguffey, M. Levin, T. T. Matsuoka, V. Chvykov, G. Kalinchenko, P. Rousseau, V. Yanovsky, A. Zigler, A. Maksimchuk, and K. Krushelnick, Phys. Plasmas **16,** 113105 (2009).

[22] Y. Ehrlich, C. Cohen, A. Zigler, J. Krall, P. Sprangle, and E. Esarey, Phys. Rev. Lett. **77,** 4186 (1996).

[23] D. Kaganovich, P. V. Sasorov, Y. Ehrlich, C. Cohen, and A. Zigler, Appl. Phys. Lett. **71,** 2925 (1997).

[24] D. Kaganovich, A. Ting, C. I. Moore, A. Zigler, H. R. Burris, Y. Ehrlich, R. Hubbard, and P. Sprangle, Phys. Rev. E **59,** R4769 (1999).

[25] S. M. Hooker, D. J. Spence, and R. A. Smith, J. Opt. Soc. Am. B **17,** 90 (2000).

[26] M. C. Marconi, C. H. Moreno, J. J. Rocca, V. N. Shlyaptsev, and A. L. Osterheld, Phys. Rev. E **62,** 7209 (2000).

[27] D. J. Spence and S. M. Hooker, Phys. Rev. E **63,** 015401 (R) (2000).

[28] N. A. Bobrova, A. A. Esaulov, J.-I. Sakai, P. V. Sasorov, D. J. Spence, A. Butler, S. M. Hooker, and S. V. Bulanov, Phys. Rev. E **65,** 016407 (2001).

[29] D. J. Spence, A. Butler, and S. M. Hooker, J. Opt. Soc. Am. B **20,** 138 (2003).

[30] A. Butler, D. J. Spence, and S. M. Hooker, Phys. Rev. Lett. **89,** 185003 (2002).

[31] W. P. Leemans, A. J. Gonsalves, H.-S. Mao, K. Nakamura, C. Benedetti, C. B. Schroeder, C. Tóth, J. Daniels, D. E. Mittelberger, S. S. Bulanov, J.-L. Vay, C. G. R. Geddes, and E. Esarey, Phys. Rev. Lett. **113,** 245002 (2014).

[32] N. A. Bobrova, P. V. Sasorov, C. Benedetti, S. S. Bulanov, C. G. R. Geddes, C. B. Schroeder, E. Esarey, and W. P. Leemans, Phys. Plasmas **20,** 020703 (2013).

[33] A. J. Gonsalves *et al.*, Phys. Plasmas **27,** 053102 (2020).

[34] C. V. Pieronek, A. J. Gonsalves, C. Benedetti, S. S. Bulanov, J. van Tilborg, J. H. Bin, J. H. Bin, K. K. Swanson, J. Daniels, G. Bagdasarov, N. Bobrova, V. Gasilov, G. Korn, P. Sasorov, C. G. R. Geddes, C. B. Schroeder, W. P. Leemans, and E. Esarey, Phys. Plasmas **27,** 093101 (2020).

[35] See Supplemental Material at http://link.aps.org/supplemental/10.1103/PhysRevAccelBeams.24.091301 for further discussion of deposition process.

[36] G. A. Bagdasarov, P. V. Sasorov, V. A. Gasilov, A. S. Boldarev, O. G. Olkhovskaya, C. Benedetti, S. S. Bulanov, A. Gonsalves, H.-S. Mao, C. B. Schroeder, J. van Tilborg, E. Esarey, W. P. Leemans, T. Levato, D. Margarone, and G. Korn, Phys. Plasmas **24,** 083109 (2017).

[37] C. Benedetti, C. Schroeder, E. Esarey, and W. Leemans, Phys. Plasmas **19,** 053101 (2012).

[38] K. Nakamura, H. Mao, A. J. Gonsalves, H. Vincenti, D. E. Mittelberger, J. Daniels, A. Magana, C. Toth, and W. P. Leemans, IEEE J. Quantum Electron. **53,** 1 (2017).

[39] A. Gonsalves, K. Nakamura, C. Lin, J. Osterhoff, S. Shiraishi, C. Schroeder, C. Geddes, C. Toth, E. Esarey, and W. Leemans, Phys. Plasmas **17,** 056706 (2010).

[40] C. Benedetti, C. Schroeder, E. Esarey, C. Geddes, and W. Leemans, AIP Conf. Proc. **1299,** 250 (2010).

[41] C. Benedetti, C. Schroeder, C. Geddes, E. Esarey, and W. Leemans, Plasma Phys. Controlled Fusion **60,** 014002 (2017).